Hindawi
Advances in Civil Engineering
Volume 2022, Article ID 2129573, 15 pages
https://doi.org/10.1155/2022/2129573

Research Article

Dynamic Response Analysis of Buried Drainage Pipes for Polymer Grouting Trenchless Rehabilitation under the Traveling Wave Effect

Fengyang Miao,[1] **Weiguo Li**,[2] **Jianguo Xu**,[1] **Zhihao Chen**,[3] **and Xiaoyu Feng**[2]

[1]*School of Water Conservancy Engineering, Zhengzhou University, Zhengzhou 450001, Henan, China*
[2]*Henan Highway Engineering Bureau Group Co. LTD, Zhengzhou 450052, Henan, China*
[3]*Zhongshui Northeast Survey Design and Research Co. LTD, Changchun 130021, Jilin, China*

Correspondence should be addressed to Jianguo Xu; jianguoxu@zzu.edu.cn

Received 6 June 2022; Accepted 18 August 2022; Published 29 September 2022

Academic Editor: Pengjiao Jia

The polymer grouting nonexcavation repair technology has been widely used in the repair of underground pipeline leaks, but the seismic response to the polymer repair pipeline is currently using a consistent excitation of seismic input without considering the influence of the traveling wave effect. This paper establishes the longitudinal and transverse vibration models of the polymer grout repair pipeline considering the traveling wave effect based on the elastic foundation beam theory. The seismic input uses artificially generated random seismic waves and solves the differential equations for pipeline vibration to carry out seismic response analysis of long-buried pipelines under three conditions: normal, vacant, and polymer grouting repair. The results show that after considering the traveling wave effect, the reaction of each measuring point on the pipeline has obvious phase characteristics, and the waveform of the distant measuring point has an obvious hysteresis phenomenon; the seismic wave velocity has a great influence on the deformation of the pipeline, and the displacement amplitude of the pipeline increases with the increase of the seismic wave velocity. The peak of pipeline displacement after vacancy will increase by 100%~300% more than normal, while the difference in pipeline deformation after high polymer grouting is about 25% compared with normal, which means that the bottom vacant will have a great influence on pipeline deformation, and high polymer repair can restore the pipeline mechanical properties to normal levels.

1. Introduction

The polymer grouting repair technology is used to fill the void, seal the leakage, and lift and settle the pipeline by injecting polymer grouting material into the leaky part of the pipeline structure, and as a minimally invasive and efficient underground pipeline trenchless repair technology, this technology has been successfully applied in many underground pipeline repair projects [1–3]. Studies have also been conducted on the seismic response of polymer-repaired pipes [4–7], but the seismic inputs used in all of these studies were consistent excitation. For small-span structures, it is reasonable not to consider the spatial variation of ground shaking. However, studies have shown that the use of seismic input with consistent excitation for large-span structures such as pipelines is not practical and may lead to unreasonable seismic design [8–11]. Therefore, it is necessary to perform a nonuniform excitation seismic response analysis for polymer grouting to repair underground drainage pipes.

The variability of ground shaking includes temporal and spatial differences, mainly traveling wave effects, local site effects, and partial coherence effects with traveling-wave effects dominating [12, 13]. Therefore, this paper will consider the dynamic response of the high polymer repair pipe under the traveling wave effect and establish the vibration equation of the high polymer repair pipe considering the traveling wave effect based on the elastic foundation beam theory. The seismic input uses artificially generated random

seismic waves and then analyzes the effect of different apparent wave speeds on the traveling wave effect.

2. Solving Vibration Equations for Polymer Repaired Pipes under the Traveling Wave Effect

As shown in Figure 1, for the dynamic response of the polymer repair pipeline under the traveling wave effect, this paper assumes the underground pipeline as an infinitely long homogeneous long beam on an elastic foundation and combines the analytical model of pipe-soil-polymer interaction previously proposed by the authors [7], neglecting the internal damping of the pipeline, to obtain a computational model of the seismic response of the polymer repair pipeline.

2.1. Solving the Longitudinal Vibration Response Equation for Pipelines. The underground continuous pipeline is usually very long, and when doing the actual calculation, you can take one of the pipe sections to calculate. When the length of the calculated pipe section is large enough, the influence of the boundary conditions on the middle part of the calculated pipe section is small, so the calculated pipe section can be regarded as a free boundary, and when the pipe generates longitudinal vibration, its calculation model and boundary conditions are shown in Figure 2.

Assuming that the medium around the underground pipe is uniformly distributed along the direction of the pipe axis, the longitudinal vibration equation of the pipe is shown as follows:

$$m\frac{\partial^2 u(x,t)}{\partial t^2} + c\frac{\partial u(x,t)}{\partial t} + ku(x,t) - \mathrm{EA}\frac{\partial^2 u(x,t)}{\partial x^2} = ku_g(x,t) + c\frac{\partial u_g(x,t)}{\partial t}, \tag{1}$$

where m is the mass of the pipe, c is the damping factor of the surrounding medium, k is the longitudinal stiffness of the surrounding medium, EA is the axial stiffness of the pipe, $u(x,t)$ is the longitudinal displacement of the pipe, and $u_g(x,t)$ is the longitudinal ground displacement.

To solve the above-given vibration equation, the proposed static displacement method [14] is used to consider the effect of the traveling wave effect, and the longitudinal displacement of the pipe in equation (1) is decomposed as shown in equation (2), which is the proposed static displacement $u^s(x,t)$ caused by the ground motion and the dynamic displacement $u^d(x,t)$ caused by the inertia and damping of the structure, respectively.

$$u(x,t) = u^s(x,t) + u^d(x,t). \tag{2}$$

The dynamic term in equation (1) is removed to obtain the proposed static displacement ordinary differential equation.

$$ku^s(x,t) - \mathrm{EA}\frac{d^2u^s(x,t)}{dx^2} = ku_g(x,t). \tag{3}$$

The general solution of the chi-square equation corresponding to equation (3) is

$$u^s(x,t) = Ae^{-\sqrt{k/EA}x} + Be^{\sqrt{k/EA}x}. \tag{4}$$

Expanding the site displacement and pipe displacement on the interval A as a cosine series leads to the special solution of equation (3) as

$$u^s(x,t) = \frac{1}{2}a_0(t) + \sum_{n=1}^{\infty}\frac{ka_n(t)}{k - \mathrm{EA}(n\pi)^2/l^2}\cos\frac{n\pi}{l}x. \tag{5}$$

Adding equations (4) and (5) and substituting the boundary conditions yields the solution of the differential equation as

$$u^s(x,t) = \frac{1}{2}a_0(t) + \sum_{n=1}^{\infty}\frac{ka_n(t)}{k - \mathrm{EA}(n\pi)^2/l^2}\cos\frac{n\pi}{l}x. \tag{6}$$

Then, the dynamic term in formula (1) is proposed, and the following equation can be obtained:

$$m\frac{\partial^2 u^d(x,t)}{\partial t^2} + c\frac{\partial u^d(x,t)}{\partial t} + ku^d(x,t) - \mathrm{EA}\frac{\partial^2 u^d(x,t)}{\partial x^2} = -m\frac{\partial u_g(x,t)}{\partial t^2}. \tag{7}$$

The dynamics of displacement can be solved by the vibration superposition method [15]. Firstly, the damping term and nonflush term in equation (7) are removed, and the self-oscillation frequency and vibration shape are obtained by substituting the boundary conditions using the separation of variables method as follows:

$$\omega_n = \sqrt{\frac{n^2\pi^2 EA}{l^2 m} + \frac{k}{m}}, \qquad \phi_n(x) = \cos\frac{n\pi}{l}x. \tag{8}$$

Then,

$$u^d(x,t) = \sum_{n=0}^{\infty} q_n(t)\phi_n(x). \tag{9}$$

Substituting the above equation into equation (7), we get

$$m\sum_{n=1}^{\infty}\frac{d^2q_n(t)}{dt^2}\cos\frac{n\pi}{l}x + c\sum_{n=1}^{\infty}\frac{dq_n(t)}{dt}\cos\frac{n\pi}{l}x + k\sum_{n=1}^{\infty}q_n(t)\cos\frac{n\pi}{l}x$$
$$-\mathrm{EA}\sum_{n=1}^{\infty}q_n(t)\left(\frac{n\pi}{l}\right)^2\cos\frac{n\pi}{l}x = -mf(t)\sum_{k=0}^{N}C_k\cos(\omega_k t+\phi_k). \tag{10}$$

Decoupling equation (10) using the vibration superposition method, we obtain

$$m\sum_{n=1}^{\infty}\frac{d^2q_n(t)}{dt^2}\cos\frac{n\pi}{l}x\cdot\cos\frac{m\pi}{l}x + c\sum_{n=1}^{\infty}\frac{dq_n(t)}{dt}\cos\frac{n\pi}{l}x\cdot\cos\frac{m\pi}{l}x + k\sum_{n=1}^{\infty}q_n(t)\cos\frac{n\pi}{l}x\cdot\cos\frac{m\pi}{l}x$$
$$-\mathrm{EA}\sum_{n=1}^{\infty}q_n(t)\left(\frac{n\pi}{l}\right)^2\cos\frac{n\pi}{l}x\cdot\cos\frac{m\pi}{l}x$$
$$= -mf(t)\sum_{k=0}^{N}C_k\cos(\omega_k t+\phi_k)\cdot\cos\frac{m\pi}{l}x. \tag{11}$$

Equation (11) is integrated over the interval (0, l), and according to the orthogonality of the vibration pattern, we get

$$m\frac{d^2q_n(t)}{dt^2} + c\frac{q_n(t)}{dt} + kq_n(t) - EAq_n\left(\frac{n\pi}{l}\right)^2 = -m\sum_{k=1}^{N}A\sin\left(\omega_k - \frac{\omega_k l}{c} + \phi_k + n\pi\right) - A\sin(\omega_k t+\phi_k)$$
$$+B\sin\left(\omega_k - \frac{\omega_k l}{c} + \phi_k - n\pi\right) - B\sin(\omega_k t+\phi_k), \tag{12}$$

where $A = 1/-\omega_k/c + n\pi/l\cdot C_k/2\omega_k^2$, $B = 1/-\omega_k/c - n\pi/l\cdot C_k/2\omega_k^2$.

Take the first N vibration types for calculation, and after finding the corresponding a, the dynamic displacement can be approximated according to equation (9).

$$u^d(x,t) \approx \sum_{n=0}^{N}q_n(t)\phi_n(x). \tag{13}$$

Finally, the proposed static displacement and dynamic displacement are summed to obtain the displacement solution of the longitudinal vibration equation of the pipe under the traveling wave effect, and the strain and internal force of the pipe can be further obtained from the displacement.

2.2. Pipeline Transverse Vibration Response Equation Solving. The pipeline transverse vibration calculation model and boundary conditions are shown in Figure 3, and the transverse vibration equation is

$$m\frac{\partial^2u(x,t)}{\partial t^2} + c\frac{\partial u(x,t)}{\partial t} + ku(x,t) + \mathrm{EI}\frac{\partial^4u(x,t)}{\partial x^4} = ku_g(x,t) + c\frac{\partial u_g(x,t)}{\partial t}. \tag{14}$$

Although the equations of motion and boundary conditions for longitudinal and transverse vibrations are different, the solution ideas are the same, so we will not repeat them here. By replacing a with b in the above longitudinal vibration, the proposed static displacement of the transverse vibration can be obtained as

$$u^s(x,t) = \frac{1}{2}a_0(t) + \sum_{n=1}^{\infty}\frac{ka_n(t)}{k+\mathrm{EI}(n\pi)^4/l^4}\cos\frac{n\pi}{l}x. \tag{15}$$

Correspondingly, its differential equation for solving a is

$$m\frac{d^2q_n(t)}{dt^2}+c\frac{q_n(t)}{dt}+kq_n(t)+EIq_n\left(\frac{n\pi}{l}\right)^4=-m\sum_{k=1}^{N}A\sin\left(\omega_k-\frac{\omega_k l}{c}+\phi_k+n\pi\right)-A\sin\left(\omega_k t+\phi_k\right)$$
$$+B\sin\left(\omega_k-\frac{\omega_k l}{c}+\phi_k-n\pi\right)-B\sin\left(\omega_k t+\phi_k\right). \tag{16}$$

3. Artificial Random Seismic Wave Generation

Since the actual seismic waves cannot match the corresponding seismic environment and site conditions, the actual seismic records are discrete and cannot be used for subsequent calculations. Therefore, the seismic wave input in this paper adopts artificially generated random seismic waves. The seismic input uses artificially generated random seismic waves, whose generation method is based on the Clough–Penzien power spectrum of a smooth ground shaking process [16], and introduces a generalized evolutionary power spectrum model of a nonsmooth ground shaking acceleration process and associated parameters. The generalized evolutionary power spectrum model fully takes into account the time-varying characteristics of the ground shaking duration, peak ground shaking acceleration, site soil circular frequency, and damping ratio, and the expression of this power spectrum density function is

$$S_a(\omega,t)=A^2(t)\frac{\omega_g^2(t)+4\xi_g^2(t)\omega_g^2(t)\omega^2}{\left(\omega^2-\omega_g^2(t)\right)^2+4\xi_g^2(t)\omega_g^2(t)\omega^2}\times\frac{\omega^4S_0(t)}{\left(\omega^2-\omega_j^2(t)^2++4\xi_j^2(t)\omega_j^2(t)\omega^2\right.},$$
$$A(t)=\left[\frac{t}{t_{\max}}\exp\left(1-\frac{t}{t_{\max}}\right)\right]^d, \tag{17}$$
$$S_0(t)=\frac{\overline{a}_{\max}^{\,2}}{\gamma^2\pi\omega_g(t)\left[2\xi_g(t)+1/2\xi_g(t)\right]},$$

where $A(t)$ is called the forced modulation coefficient, $t_{\max}$ is the moment corresponding to the peak acceleration, d is the modulation coefficient shape control index, $S_0(t)$ is the spectral parameter indicating the ground vibration intensity, $\overline{a}_{\max}$ is the average peak acceleration, and γ is the equivalent peak factor. $\omega_g(t),\xi_g(t)$ are the site soil self-oscillation circle frequency and damping ratio, respectively; $\omega_j(t),\xi_j(t)$ are the filtering parameters. Site parameters and filtering parameters are linear functions of time, respectively.

For a zero-mean nonsmooth ground shaking acceleration time series $a(t)$, if its evolutionary power spectral density function is $S_a(\omega_i,t)$, the nonsmooth earthquake acceleration time series can be modeled as

$$a(t)=\sum_{i=1}^{N}\sqrt{S_a(\omega_i,t)\Delta\omega}\left[\cos(\omega_i t)X_i+\sin(\omega_i t)Y_i\right]. \tag{18}$$

The calculated response spectrum $S_a(\omega,\zeta)$ can be approximated to the design response spectrum $S_a^T(\omega,\zeta)$ by iterative correction of the amplitude spectrum according to equation (19) using the numerical analysis software calculation program.

$$S_a^{i+1}(\omega_k,t)=S_a^i(\omega_k,t)\cdot\left[\frac{S_a^T(\omega_k,\zeta)}{S_a(\omega_k,\zeta)}\right]^2. \tag{19}$$

The evolving power spectrum density function $S_a(\omega,t)$ used in this paper can be determined from the standard response spectrum of hydraulic design, and the relevant parameters can be determined according to SL203-97 "Code for Seismic Design of Hydraulic Buildings" [14]. Then, the artificial seismic waves generated based on the above process are shown in Figure 4.

4. Analysis of Calculation Results

Based on the above solution process, a calculation program was prepared using numerical analysis software, and the calculation and analysis of the example were carried out. For the calculation, the length of the pipe is 1000 m, and three measurement points are selected at 200 m, 500 m, and 800 m along the pipe axis to analyze the deformation of the pipe under normal, vacant, and repair conditions [17, 18]. A vacant is assumed to occur at the bottom of the entire pipe (approximately 1/8 of the circular area of the entire pipe), along the direction of the pipe axis, through the entire bottom of the pipe [3].

The standard spectrum of artificial random seismic wave design is determined according to SL203-97 "Seismic Design Code for Hydraulic Buildings," and the loading direction is divided into two directions: longitudinal and transverse [14]. Although the propagation velocity of seismic waves in soft soil is generally 50 m/s~250 m/s, the propagation velocity of

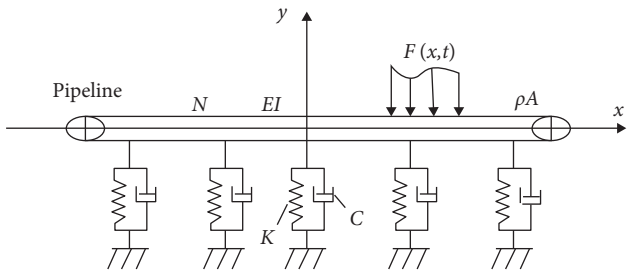

Figure 1: Seismic response calculation model for polymer rehabilitation pipeline.

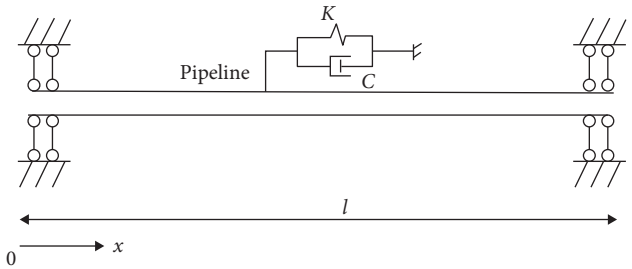

Figure 2: Pipeline longitudinal vibration calculation model and boundary conditions.

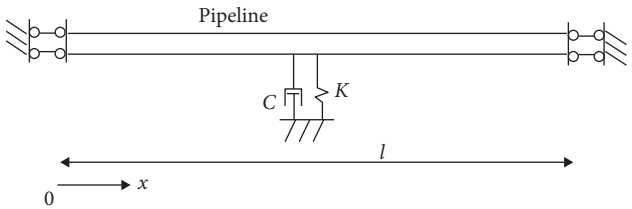

Figure 3: Pipeline transverse vibration calculation model and boundary conditions.

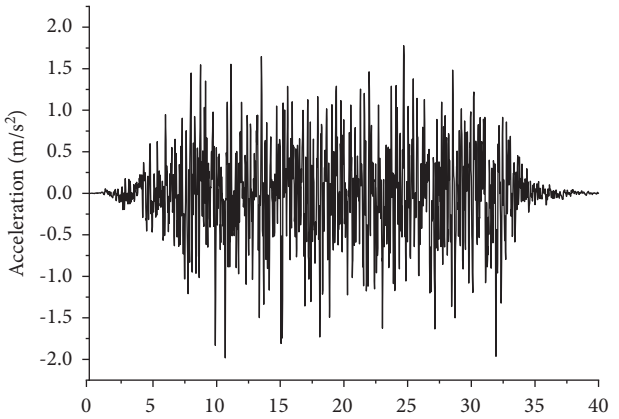

Figure 4: Artificial seismic waves generated using numerical analysis software.

seismic waves increases with the increase of soil depth [19, 20], and the propagation velocity in bedrock increases significantly, reaching 2000 m/s~2500 m/s [21, 22]. The basic

Table 1: The basal apparent wave velocity of the EI-Centro station.

Depth/ m	Thickness (m)	Soil	Apparent wave velocity (m/s)
4.2	4.2	Clay	122
5.6	1.2	Sand clay	122
15.7	10.1	Sandy clay-silting clay	175
21.8	6.1	Sand silt clay	213
34.8	13.0	Fine sand soil	251
42.3	7.5	Silted clay	251
45.9	3.6	Silt fine sand	251
65.5	19.6	Silted clay	305
68.5	13.0	Silt fine sand	—

Table 2: Calculated stiffness values for normal, vacant, and repair conditions.

Work conditions	Calculated stiffness (10^7 N/m^2)	
	Longitudinal vibration	Transverse vibration
Normal	7.13	6.33
Vacant	8.94	8.01
Polymer grouting repair	6.04	5.97

apparent wave velocity of the EI-Centro wave station is shown in Table 1 in the manuscript. Therefore, three-wave velocities of 100 m/s, 200 m/s, and 500 m/s are used to analyze the seismic waves in this paper.

The values of the medium stiffness around the pipe in the vibration equation under normal, vacant, and repair conditions can be calculated according to the equations in the previous research results [7], and the specific data can be found in Table 2, and for space reasons, the detailed solution process will not be repeated. The damping is viscous damping, and the damping ratio taken in this paper is 0.05.

4.1. Analysis of Calculation Results of Longitudinal Vibration of Pipes. Figure 5 shows the comparison of the maximum values of the longitudinal vibration displacement at the three corresponding observation points for different seismic wave velocities under three working conditions, namely, normal, decoupled, and repaired. From Figure 5(b), it can be seen that the maximum values of pipe displacements at different locations do not differ much under the action of the same seismic wave. The maximum value of displacement at the 500 m measurement point is 21.012 mm when the wave speed is 500 m/s under the vacant condition, compared with 14.461 mm at the 200 m measurement point and 15.338 mm at the 800 m measurement point. The difference is 6.551 mm and 5.674 mm, respectively, and the difference is the largest at this time, and the difference is between 1 and 4 mm for the rest of the working conditions.

For the same measurement point, when the seismic wave velocity is different, the maximum value of its longitudinal vibration displacement increases with the increase of wave

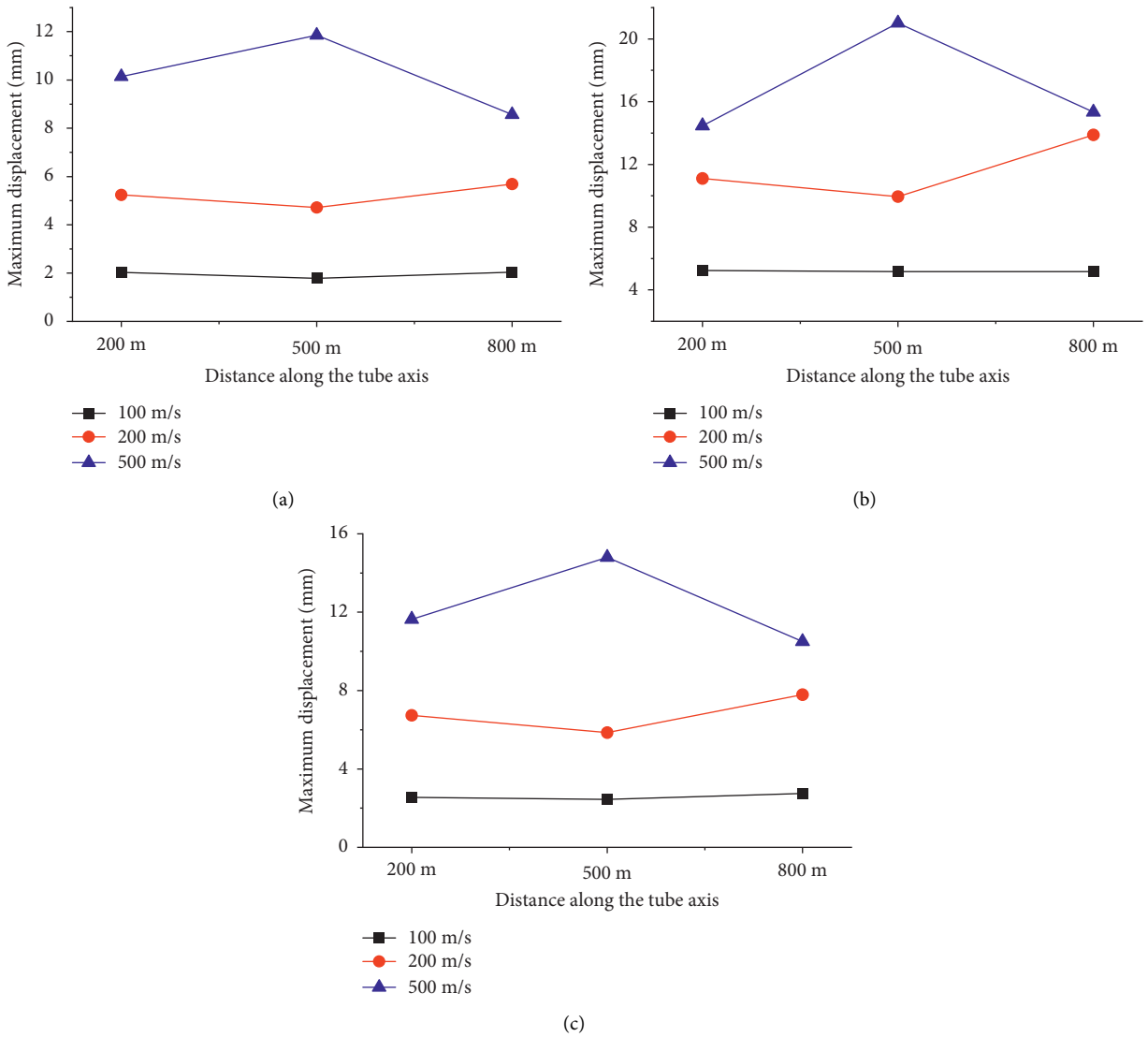

Figure 5: Maximum value of longitudinal vibration displacement of the pipeline under different wave velocities. (a) Normal, (b) vacant, and (c) polymer grouting repair.

velocity. From Figure 5(a), it can be seen that the maximum values of pipe displacement at 200 m of the measurement point under normal conditions are 2.030 mm, 5.240 mm, and 10.139 mm with the increase of seismic wave velocity, and the maximum values of displacement at wave velocity 200 m/s and wave velocity 500 m/s are increased by 2.58 times and 4.99 times, respectively, compared with that at wave velocity 100 m/s. Similarly, from Figure 5(c), it can be seen that the maximum values of displacement at 200 m after repair are 2.548 mm, 6.733 mm, and 11.634 mm, respectively, which are 2.64 times and 4.56 times higher compared to the wave speed of 100 m/s.

As can be seen from Figure 5, the displacement maximum value of the pipeline increases significantly for the pipeline vacant case relative to the normal burial condition of the pipeline. For example, at the 500 m measurement point, the displacement maxima of the decoupled pipe at wave velocities of 100 m/s, 200 m/s, and 500 m/s increased by 3.374 mm, 5.226 mm, and 9.156 mm, respectively, compared with normal conditions. The displacement maxima of the repaired pipeline are small compared with the normal condition. At the 500 m measurement point, the displacement maxima of the repaired pipeline with polymer are 2.442 mm, 5.856 mm, and 14.793 mm, respectively, and the errors are 20%, 21%, and 13%, respectively, compared with the displacement maxima under normal conditions at the same wave speed, which are small. From the above analysis, it can also be seen that the vacant has a greater impact on the pipeline, which will make the seismic response of the pipeline increase significantly, and the maximum value of the pipeline displacement will be significantly reduced after the repair by polymer deformation close to the longitudinal displacement deformation of the normally buried pipeline, reflecting the repair effect of polymer grouting on the pipeline vacant.

Figure 6 shows the comparison of the longitudinal vibration displacement time curves of the pipe at different positions. As can be seen from Figure 6, the trend of the

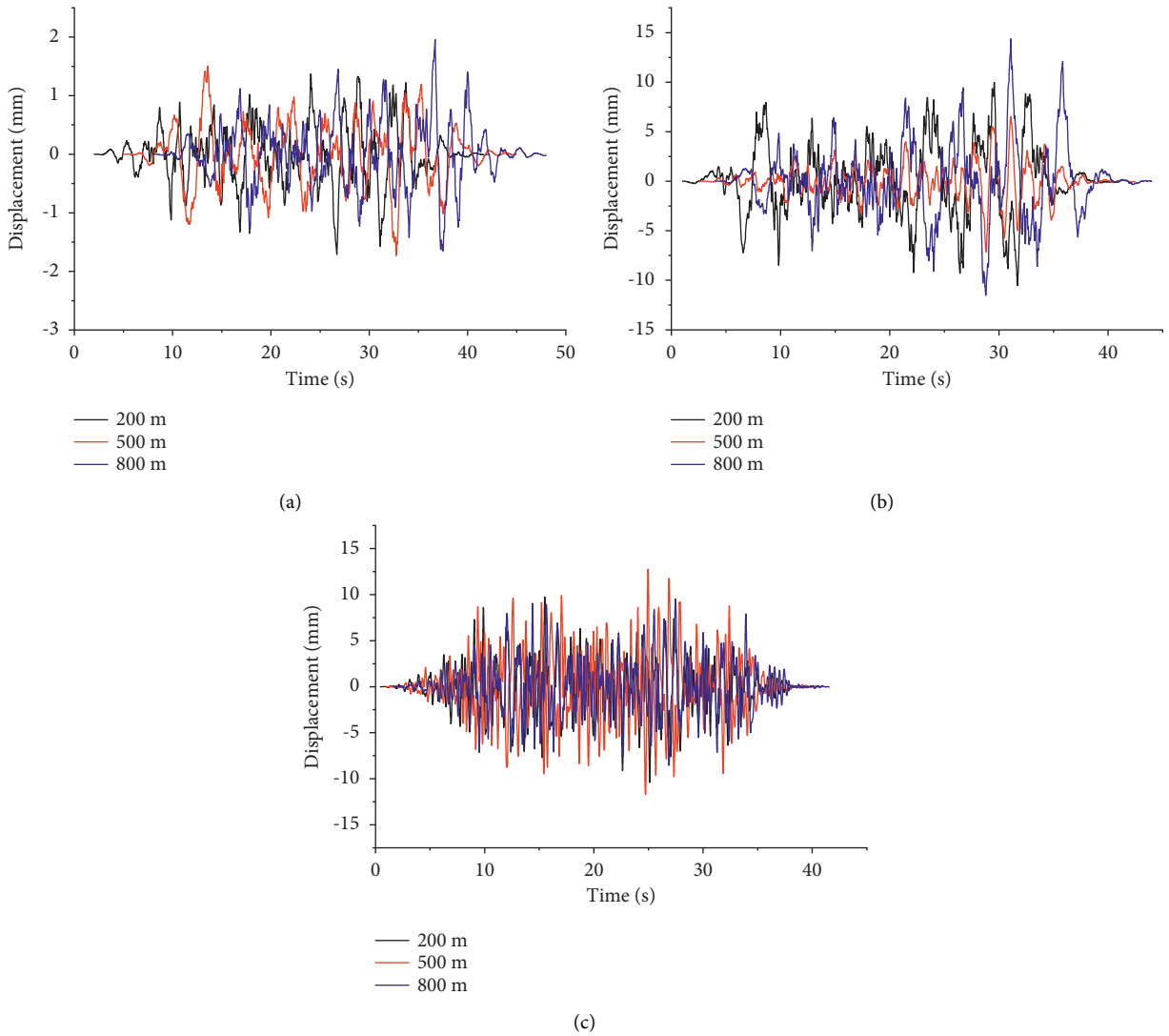

Figure 6: Longitudinal vibration displacement time course curves of pipes at different positions. (a) Wave speed $v = 100$ m/s (normal). (b) Wave speed $v = 200$ m/s (vacant). (c) Wave speed $v = 500$ m/s (polymer grouting repair).

displacement time curve at different locations of the pipeline under normal, vacant, and repair conditions under the same seismic action is basically the same, while the response of each measurement point of the pipeline has obvious phase characteristics. From Figure 6(a), it can be seen that when the wave speed is 100 m/s, the displacement time curve at the measurement point 800 m has a significant lag relative to that at 200 m, and the lag time is approximately equal to the propagation time of the seismic wave between the two. This hysteresis can also be seen in Figure 6(b) for a wave speed of 200 m/s. This hysteresis is not obvious in Figure 6(c) due to the faster wave speed, which is in general agreement with the results obtained in the literature [23]. From Figure 6, it can be seen that the peak values of pipes at different locations are slightly different for the same seismic wave velocity. This is because the length of pipes used in the actual calculation is taken as a constant value compared to the theoretical assumption of infinite length pipes, which cannot eliminate the effect of boundary effects.

Figure 7 shows the comparison of the longitudinal vibration displacement time curves of the pipe at the same position under different wave velocity conditions. From Figure 7, it can be obtained that the displacement time curves at the same location of the pipeline under normal, vacant, and repair conditions are basically of the same waveform under different wave velocity conditions, and the displacement amplitude increases with the increase of seismic wave velocity. Figure 7(a) shows the displacement time curve at 200 m under the normal condition, and the displacement maximum increases by 392% and 56% with increasing wave speed, and the displacement maximum increases by 307% and 111% at 500 m in Figure 7(b) under

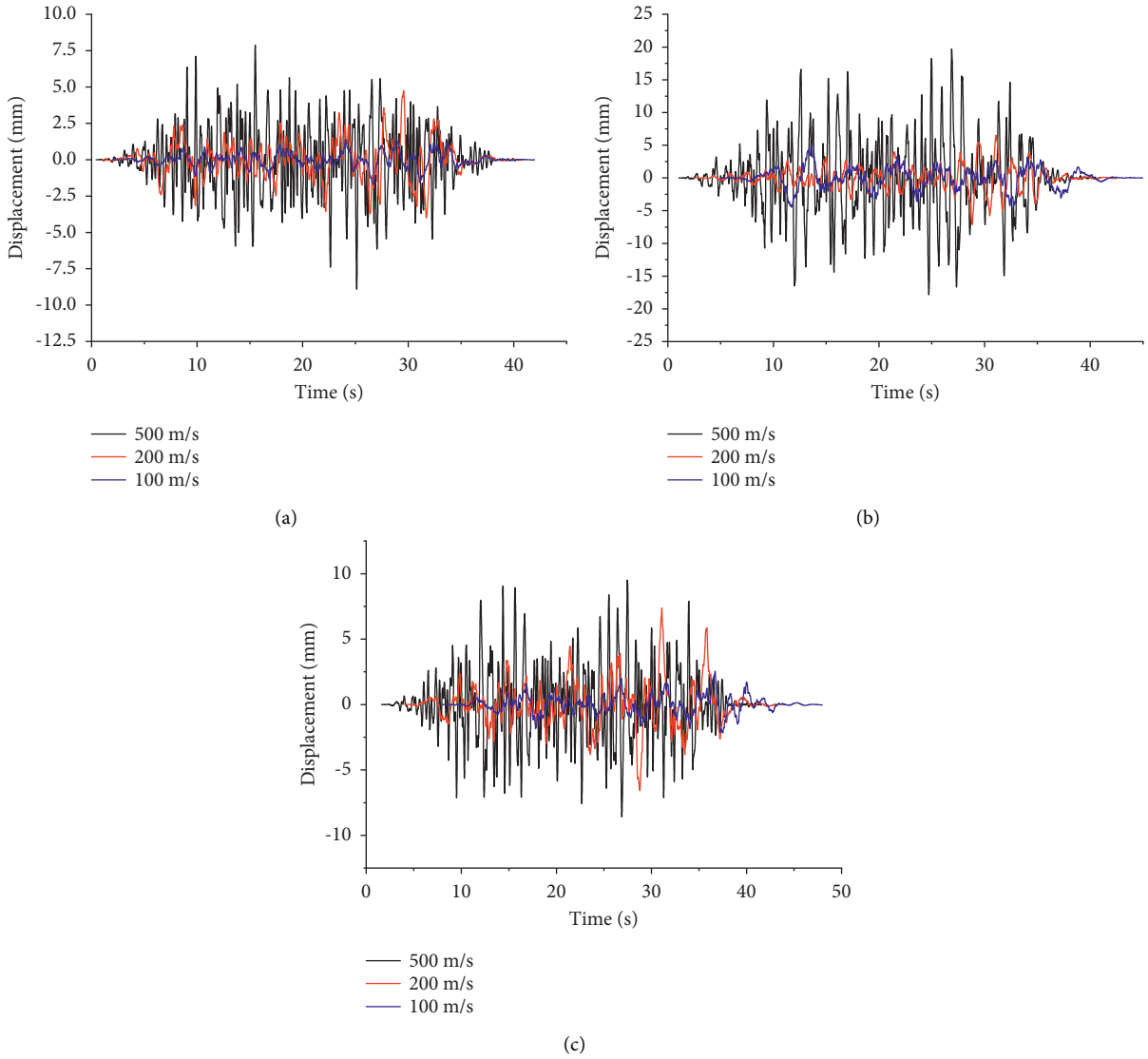

Figure 7: Longitudinal vibration displacement time curve of the pipeline under different wave velocity conditions. (a) Displacement time course curve at 200 m (normal). (b) Displacement time course curve at 500 m (vacant). (c) Displacement time course curve at 800 m (polymer grouting repair).

the vacant condition, and Figure 7(c) shows the displacement time curve at 800 m after restoration, which increases by 281% and 34% relative to 2.752 mm at 100 m/s and 200 m/s at 7.789 mm, an increase of 281% and 34%. It can be seen that after considering the traveling wave effect, the seismic wave velocity has a greater influence on the deformation of the pipeline.

Figure 8 shows the comparison of the longitudinal vibration displacement time curves of the pipe at the same position under three conditions: normal, vacant, and repaired. As can be seen from 8, the displacement amplitude of the dehollowed pipe will increase significantly compared to the normal condition at different locations and under different wave speed conditions, while the displacement value of the pipe will return to the normal level after repair. Figure 8(a) shows the comparison of normal, vacant, and repaired displacement time curves at 800 m measurement point at wave speed 100 m/s. It can be seen that the displacement value of the pipe will increase overall after being vacant, and its maximum value appears at 36.7 s as 5.164 mm, at which time the displacement is 1.993 mm under the normal condition and 2.494 mm after being repaired. Compared with the normal condition, the displacement of the dehollowed pipe increases compared with the normal situation, the displacement of the decoupled pipe increases by 159%, and the displacement of the repaired pipe only increases by 25%. As shown in Figure 8(b), when the wave speed is 200 m/s, the maximum value of the displacement of the decoupled pipe at the 500 m measurement point occurs at 31.1 s as 6.975 mm, compared with the normal situation (displacement maximum value of 3.133 mm), the

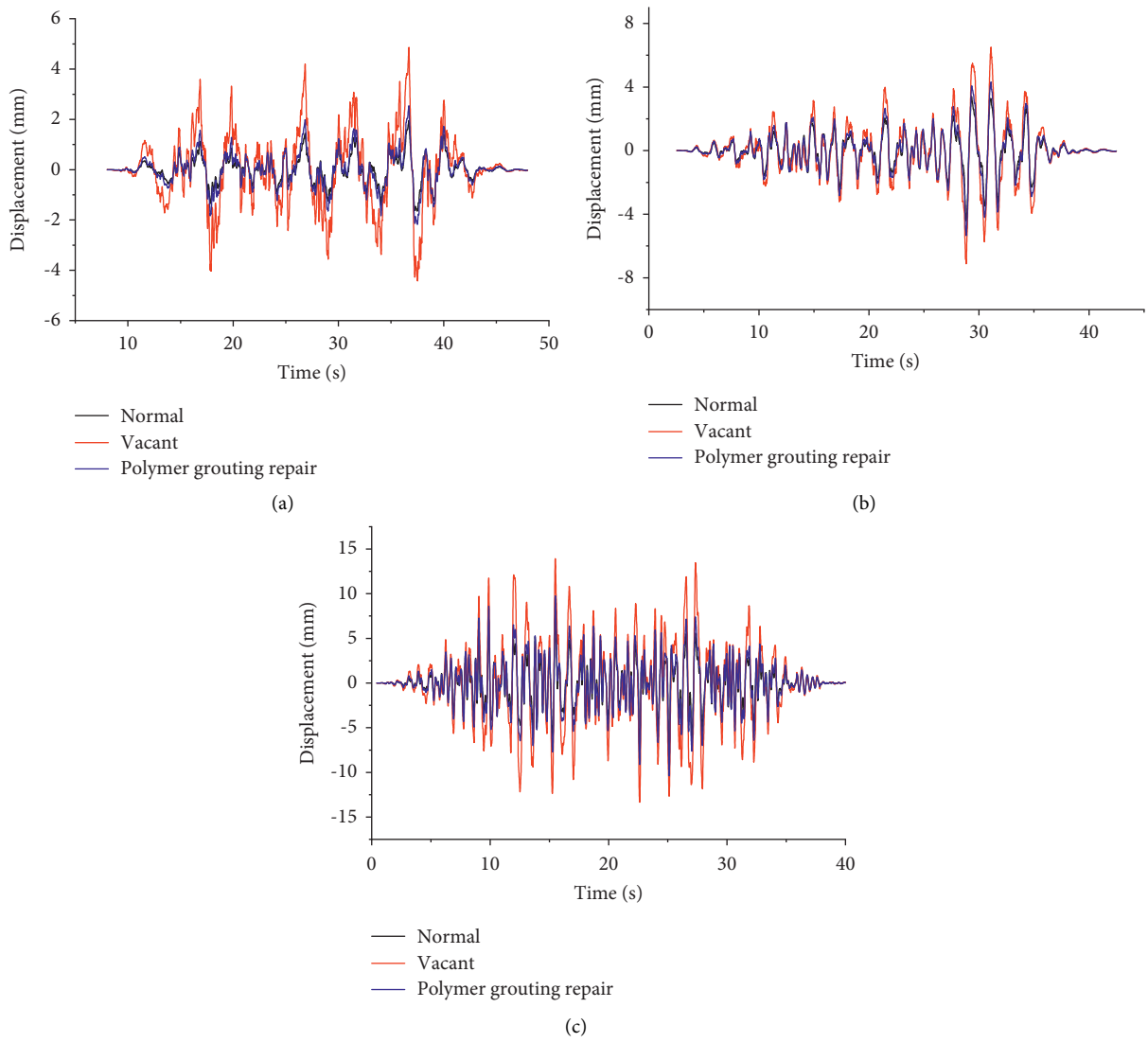

Figure 8: Longitudinal vibration displacement time curve of the pipe under normal, vacant, and polymer grouting repair. (a) At 800 m, wave speed $v = 100$ m/s. (b) At 500 m, wave speed $v = 200$ m/s. (c) At 200 m, wave speed $v = 500$ m/s.

displacement of the decoupled pipe increases by 123%, and the displacement of the repaired pipe (displacement maximum value of 4.352 mm) increases by 38%. Also, in Figure 8(c), the displacement of the dehollowed pipe is maximum at 15.6 s, 7.432 mm, at which time the displacement of the dehollowed pipe increases by 83% compared to the normal condition (displacement maximum of 4.045 mm), and the displacement of the repaired pipe (displacement maximum of 4.352 mm) increases by 7%. This shows that the bottom vacant will have a great influence on the deformation of the pipeline, and the deformation of the pipeline as a whole will increase under the vacant condition, while the deformation of the pipeline after polymer grouting will only increase by about 20% compared with the normal burial condition, bringing the deformation of the pipeline close to returning to the normal level.

4.2. Analysis of Pipeline Transverse Vibration Calculation Results. Figure 9 shows the comparison of the maximum values of transverse vibration displacement at the three measurement points for different seismic wave velocities under three working conditions, namely, normal, decoupled, and repaired. As in Figure 5, it can be seen that under the transverse vibration conditions, the displacement maximum value at the three measurement points changes basically the same law as the longitudinal vibration. Under the same seismic wave action, as shown in Figure 9(b), the maximum value of displacement at the 500 m measurement point is 37.462 mm when the wave speed is 500 m/s under repair conditions, compared with 27.618 mm at the 200 m measurement point and 26.423 mm at the 800 m measurement point; the difference is 9.834 mm and 11.039 mm, respectively, at which time the difference is the maximum. The rest of the

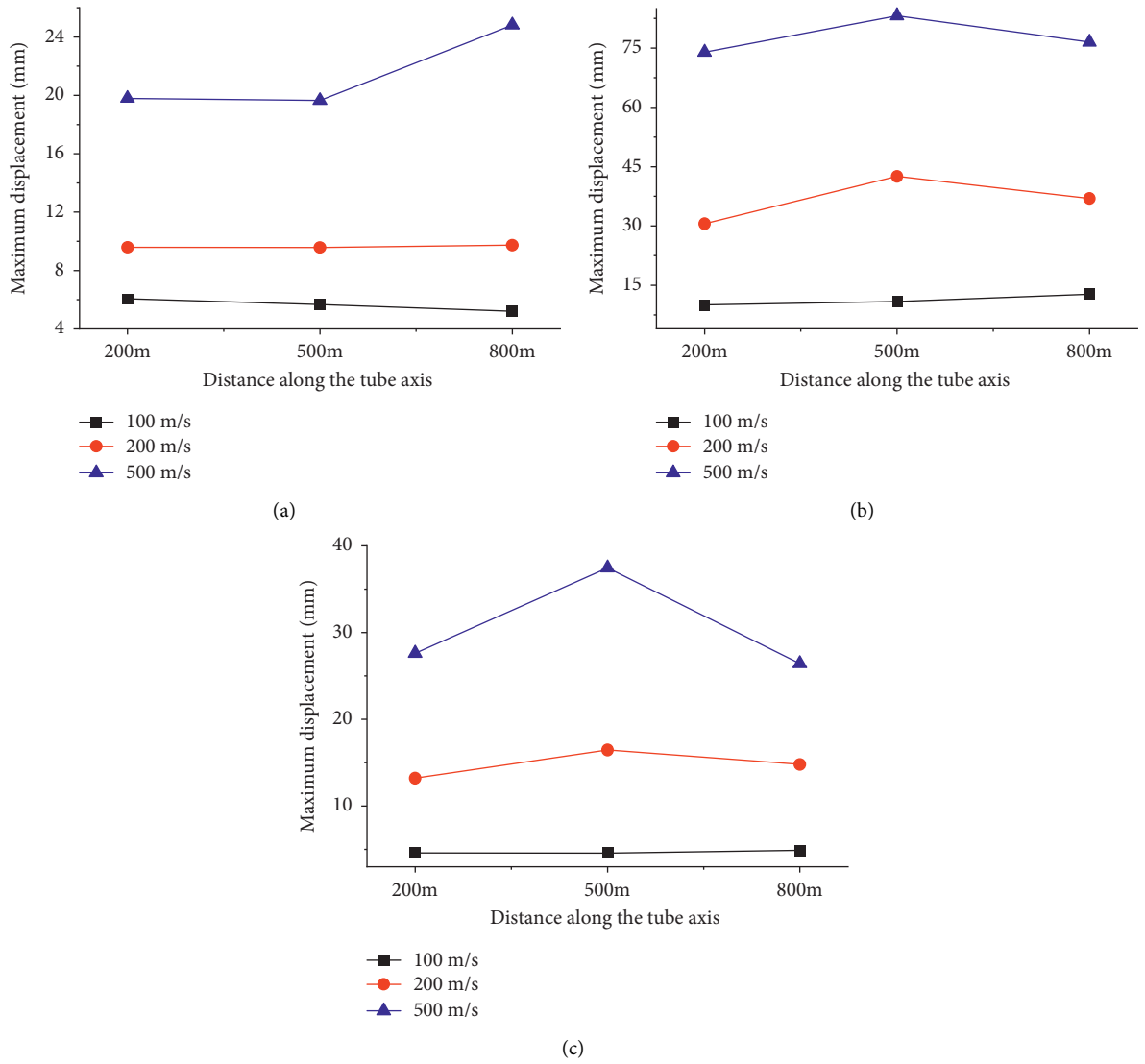

Figure 9: Maximum value of transverse vibration displacement of the pipeline under different wave velocities. (a) Normal, (b) vacant, and (c) polymer grouting repair.

working condition difference values are between 1 and 7 mm, and the maximum value of pipe displacement at different positions is not much different. For the same measurement point, when the seismic wave velocity is different, the maximum value of its longitudinal vibration displacement increases with the increase of wave velocity. The vacant has a greater impact on the pipeline, which will cause a significant increase in the maximum value of the pipeline displacement. After repair by polymer, the maximum value of the pipeline displacement will be significantly reduced, the error will be smaller compared with the normal condition, and the deformation will be close to the deformation in normal use.

Figure 10 shows the comparison of the time course curves of transverse vibration displacement of the pipeline at different locations. From Figure 10, it can be seen that the time course curves of transverse vibration displacement at different locations of the pipeline under normal, vacant, and repair conditions under the action of the same earthquake also have basically the same trend, while the response of each measurement point of the pipeline has the same phase characteristics as the longitudinal vibration. From Figure 10(a), it can be seen that this hysteresis phenomenon is most obvious when the wave speed is 100 m/s. In Figure 10(c), the waveforms at different locations roughly overlap when the wave speed is 500 m/s, which shows that the hysteresis phenomenon becomes less and less obvious as the wave speed increases.

Figure 11 shows the comparison of the time course curves of transverse vibration displacement of the pipeline under different wave velocity conditions at the same location. It can be seen from the figure that the transverse vibration displacement amplitude of the pipe increases with the increase of seismic wave speed. Figure 11(c)

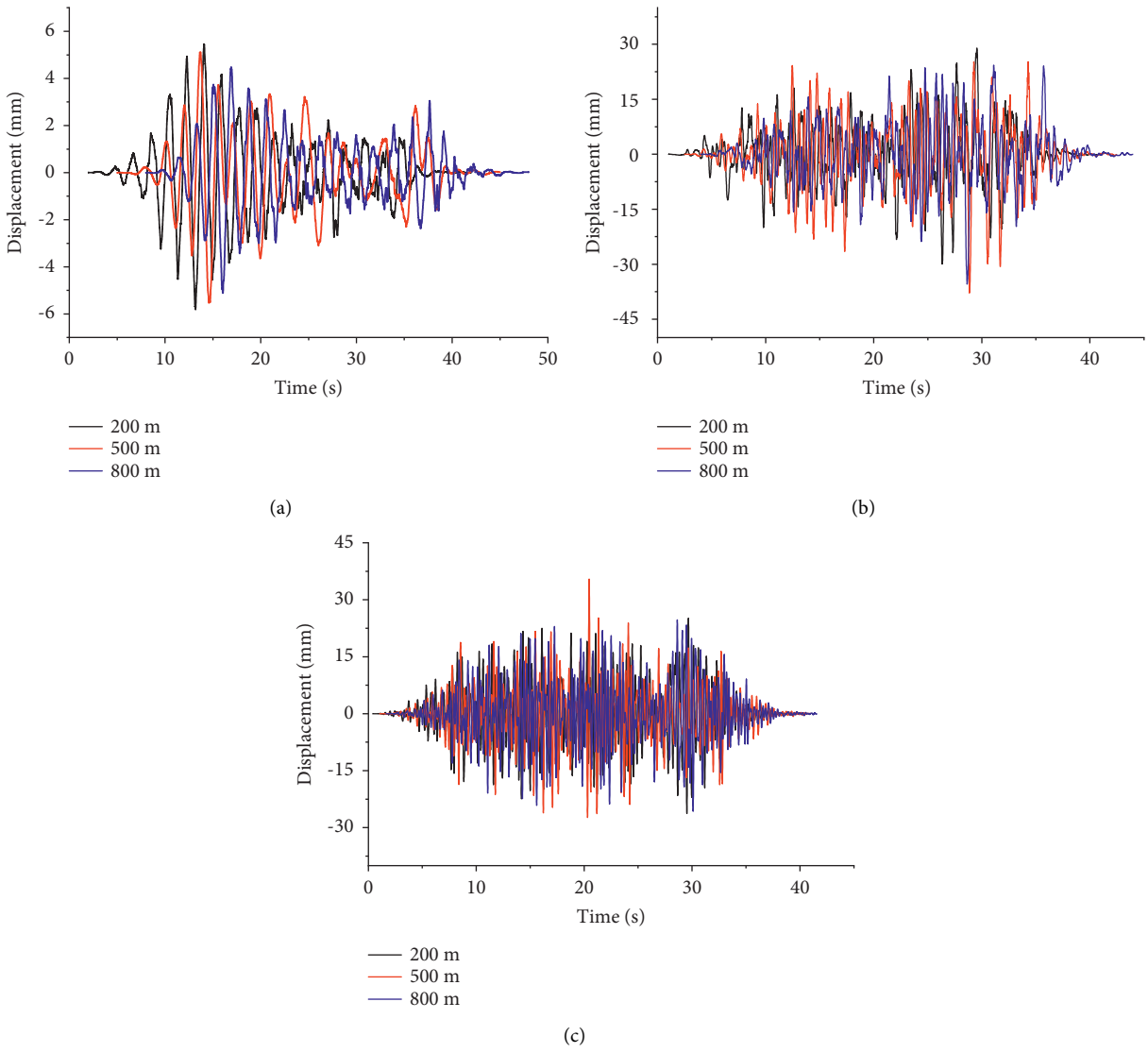

Figure 10: Time course curve of transverse vibration displacement of pipes at different positions. (a) Wave speed $v = 100$ m/s (normal). (b) Wave speed $v = 200$ m/s (vacant). (c) Wave speed $v = 500$ m/s (polymer grouting repair).

shows the displacement time course curve at 800 m after repair. The peak seismic displacement is the largest when the wave speed is 500 m/s, and the maximum displacement value is 26.423 mm at this time, which increases by 438% and 131% compared to 4.907 mm at 100 m/s and 11.403 mm at 200 m/s, respectively. Similarly, Figure 11(a) shows the displacement time curve at 200 m in the normal case with 257% and 166% increase in the displacement maximum and 717% and 166% increase in the displacement maximum at 500 m in Figure 11(b) in the off-air case. It can be seen that the seismic wave velocity has a large effect on the lateral deformation of the pipeline after considering the traveling wave effect.

Figure 12 shows the comparison of the lateral vibration displacement time curves of the pipe at the same position under normal, dehollowed, and repaired conditions. From Figure 12, it can be seen that the displacement amplitude of the dehollowed pipe increases significantly compared with the normal condition at different positions and different wave velocities, while the displacement value of the rehabilitated pipe returns to the normal level. Figure 12(a) shows the comparison of normal, vacant, and repaired displacement time curves at 800 m measurement point at wave speed 100 m/s. It can be seen that the displacement value of the pipe will increase overall after being vacant, and its maximum value appears at 12.541 mm at 36.7 s, at which time the displacement is 3.993 mm under the normal condition and 4.913 mm after being repaired. Compared with the normal condition, the displacement of the dehollowed pipe increases compared with the normal situation, the displacement of the decoupled pipe increased by 214%, and the displacement of the repaired pipe increased by 23%. As shown in Figure 12(b), when the wave speed is 200 m/s, the maximum value of the displacement

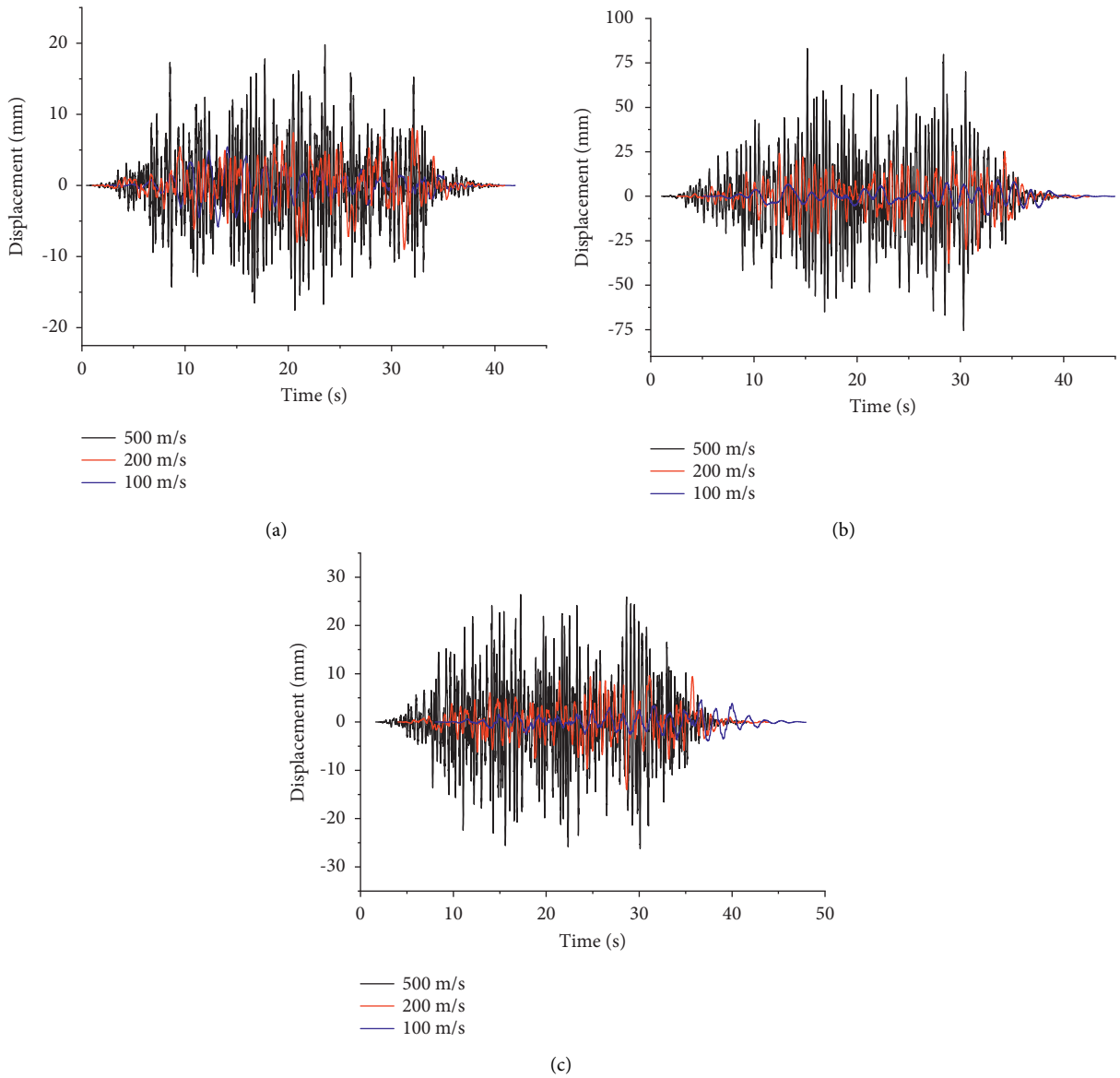

Figure 11: Time course curve of transverse vibration displacement of the pipeline under different wave velocity conditions. (a) At 200 m (normal). (b) At 500 m (vacant). (c) At 800 m (polymer grouting repair).

of the decoupled pipe at the 500 m measurement point appears at 28.8 s as 42.557 mm, at which time the displacement of the decoupled pipe increases by 193% compared with the normal situation (displacement maximum value of 14.506 mm), and the displacement of the repaired pipe (displacement maximum value of 11.805 mm) increases by 18%. Similarly, in Figure 12(c), the displacement of the dehollowed pipe is maximum at 24.8 s, which is 72.459 mm, at which time the displacement of the dehollowed pipe increases by 302% compared with the normal condition (displacement maximum is 18.013 mm), and the displacement of the repaired pipe (displacement maximum is 24.352 mm) increases by 35%. It shows that the bottom of the vacant will have a great influence on the deformation of the pipe, and the overall deformation of the pipe will increase under the vacant condition, while polymer grouting can make the deformation of the pipe basically return to the normal level.

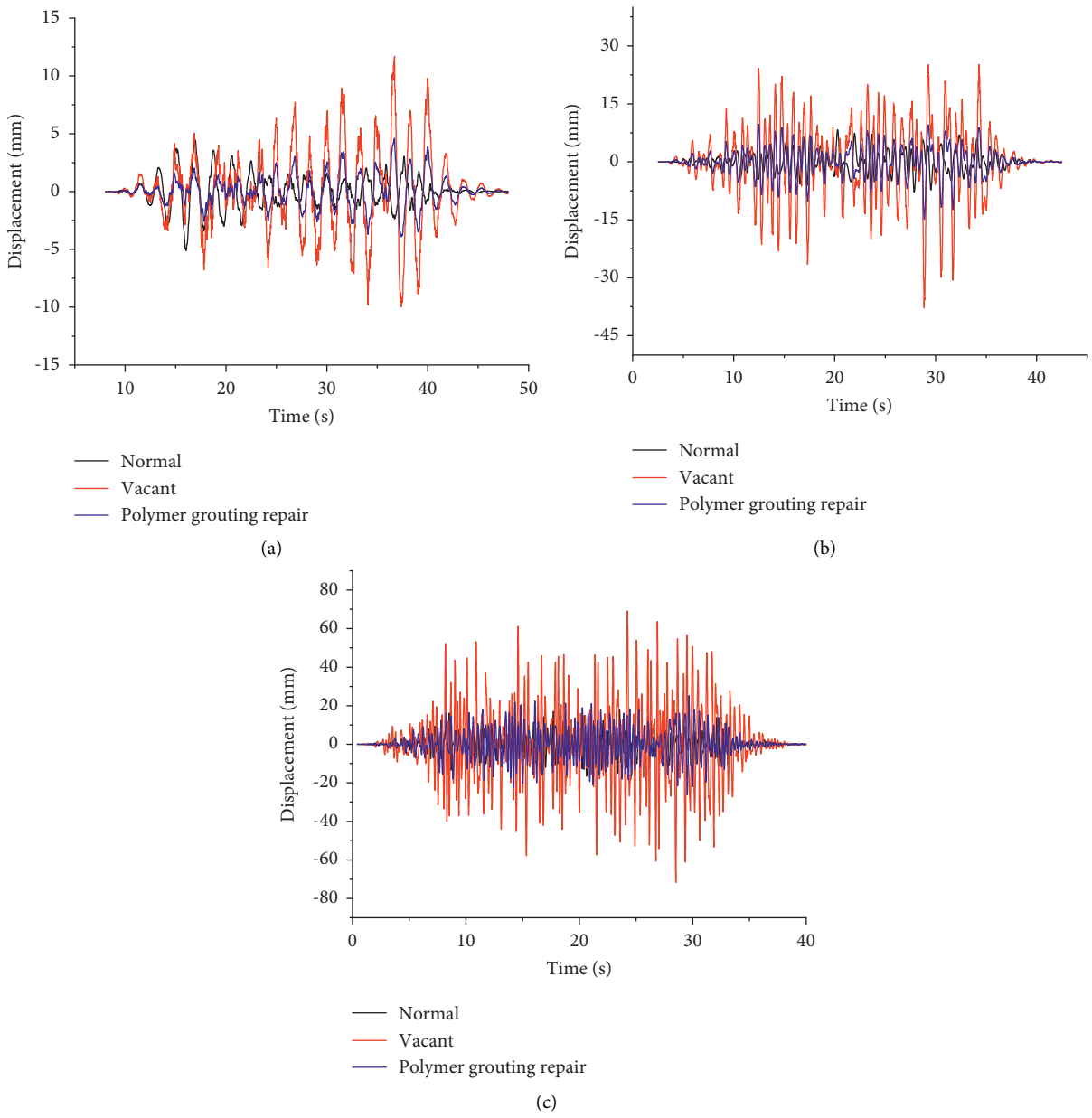

Figure 12: Time course curves of transverse vibration displacement of pipes under normal, vacant, and polymer grouting repair. (a) At 800 m, wave speed $v = 100$ m/s. (b) At 500 m, wave speed $v = 200$ m/s. (c) At 200 m, wave speed $v = 500$ m/s.

5. Conclusion

In this paper, the underground pipeline is assumed to be an infinitely long homogeneous long beam on an elastic foundation, and the seismic response calculation model of the polymer repair pipeline is established by combining the proposed analytical model of pipe-soil-polymer interaction and neglecting the internal damping of the pipeline, while the longitudinal and transverse vibration equations of the pipeline are solved by using the vibration superposition method, and finally, based on the above solution process, artificial random seismic waves are input to carry out the analysis of the seismic response of the pipeline under the traveling wave effect. The seismic response analysis of pipeline polymer repair under the effect of traveling waves was carried out based on the above solution process and inputting artificial random seismic waves. The following conclusions were obtained.

(1) Under the action of the same seismic wave, the trend of the displacement time curve at different locations of the pipeline under normal, vacant, and repair conditions is basically the same, and the difference between the maximum value of positive displacement and the maximum value of negative displacement of the pipeline at different locations is not large. At the same time, the response of each measurement point of the pipeline has obvious phase

characteristics, and the waveform of the measurement point at a farther distance has an obvious hysteresis phenomenon, but with the increase of wave speed, the hysteresis phenomenon becomes less and less obvious.

(2) The displacement time curves at the same location of the pipeline under normal, decoupled, and repaired conditions are basically the same under different wave velocities, and the displacement amplitude increases with the increase of seismic wave velocity. After considering the traveling wave effect, the seismic wave speed has a greater influence on the deformation of the pipeline.

(3) The displacement amplitude of the dehollowed pipe will increase significantly compared with the normal condition under different positions and different wave speed conditions, while the maximum displacement value of the repaired pipe basically returns to the normal level. The peak displacement of the pipe after being vacant will increase by 100%~300% compared with the normal condition, while the deformation of the pipe after polymer grouting will only increase by about 20% compared with the normal condition. It can be concluded that the bottom vacant will have a great influence on the deformation of the pipe, and the pipe deformation can be nearly restored to the normal level after the repair of polymer grouting.

Data Availability

The data presented in this study are available within the main text of the article.

Conflicts of Interest

The authors declare that they have no conflicts of interest regarding the publication of this paper.

Acknowledgments

This work was funded by the Natural Science Foundation of China (grant no. 52079128) and Science and Technology Project of Henan Province (grant no. 212102310289).

References

[1] M. S. Shi, F. M. Wang, and J. Luo, "Compressive strength of polymer grouting material at different temperatures," *Journal of Wuhan University of Technology*, vol. 25, no. 6, pp. 962–965, 2010.

[2] S. Mohammadi Esfarjani and M. Salehi, "Inspection of aboveground pipeline using vibration responses," *Journal of Pipeline Systems Engineering and Practice*, vol. 11, Article ID 04020021, 3 pages, 2020.

[3] R. Wang, F. Wang, J. Xu, Y. Zhong, and S. Li, "Full-scale experimental study of the dynamic performance of buried drainage pipes under polymer grouting trenchless rehabilitation," *Ocean Engineering*, vol. 181, pp. 121–133, 2019.

[4] M. H. Hajmohammad, M. Maleki, and R. Kolahchi, "Seismic response of underwater concrete pipes conveying fluid covered with nano-fiber reinforced polymer layer," *Soil Dynamics and Earthquake Engineering*, vol. 110, pp. 18–27, 2018.

[5] S. Alzabeebee, "Seismic response and design of buried concrete pipes subjected to soil loads," *Tunnelling and Underground Space Technology*, vol. 93, Article ID 103084, 2019.

[6] M. S. Zarei, R. Kolahchi, M. H. Hajmohammad, and M. Maleki, "Seismic response of underwater fluid-conveying concrete pipes reinforced with SiO2 nanoparticles and fiber reinforced polymer (FRP) layer," *Soil Dynamics and Earthquake Engineering*, vol. 103, pp. 76–85, 2017.

[7] J. g. Xu, Z. h. Chen, and R. Wang, "Mechanical characteristic analysis of buried drainage pipes after polymer grouting trenchless rehabilitation," *Advances in Civil Engineering*, vol. 2021, Article ID 6679412, 14 pages, 2021.

[8] L. I. Zhengying, M. U. Dejian, and D. Pengpeng, "Influence of traveling wave effect on passive seismic control of long-span bridge," *Procedia Engineering*, vol. 14, pp. 2307–2314, 2011.

[9] P. Zhang, Y. Wang, and G. Qin, "Fuzzy damage analysis of the seismic response of a long-distance pipeline under a coupling multi-influence domain," *Energies*, vol. 12, no. 1, p. 62, 2018.

[10] Z. h. Zong, R. Zhou, X. y. Huang, and Z. h. Xia, "Seismic response study on a multi-span cable-stayed bridge scale model under multi-support excitations. Part I: shaking table tests," *Journal of Zhejiang University - Science*, vol. 15, no. 5, pp. 351–363, 2014.

[11] B. Yan and G. Dai, "Seismic pounding and protection measures of simply-supported beams considering interaction between continuously welded rail and bridge," *Structural Engineering International*, vol. 23, no. 1, pp. 61–67, 2013.

[12] W. Xie, L. Sun, and M. Lou, "Shaking table test verification of traveling wave resonance in seismic response of pile-soil-cable-stayed bridge under non-uniform sine wave excitation," *Soil Dynamics and Earthquake Engineering*, vol. 134, Article ID 106151, 2020.

[13] J. B. Dai, G. D. Zhang, C. T. Hu, and K. K. Cheng, "Study on synthesis method of multipoint seismic waves for buried oil and gas pipeline in shaking table tests," *Shock and Vibration*, vol. 2021, Article ID 4624871, 8 pages, 2021.

[14] E. L. Wilson, *Three Dimensional Static and Dynamic Analysis of Structures: A Physical Approach with Emphasis on Earthquake Engineering*, Computers and Structures Incorporated, Walnut Creek, CA, USA, 1998.

[15] T. Itoh, "Damped vibration mode superposition method for dynamic response analysis," *Earthquake Engineering & Structural Dynamics*, vol. 2, no. 1, pp. 47–57, 1973.

[16] R. W. Clough and J. Penzien, *Dynamics of Structures*, pp. 121–133, McGraw-Hill, New York, 1975.

[17] D. Covas, H. Ramos, and A. B. De Almeida, "Standing wave difference method for leak detection in pipeline systems," *Journal of Hydraulic Engineering*, vol. 131, no. 12, pp. 1106–1116, 2005.

[18] H. Shamloo and A. Haghighi, "Leak detection in pipelines by inverse backward transient analysis," *Journal of Hydraulic Research*, vol. 47, no. 3, pp. 311–318, 2009.

[19] K. L. Wen, "Non-linear soil response in ground motions," *Earthquake Engineering & Structural Dynamics*, vol. 23, no. 6, pp. 599–608, 1994.

[20] E. Şafak, "Local site effects and dynamic soil behavior," *Soil Dynamics and Earthquake Engineering*, vol. 21, no. 5, pp. 453–458, 2001.

[21] A. M. Chandler, N. T. K. Lam, H. H. Tsang, and M. N. Sheikh, "Estimation of near-surface attenuation in bedrock for

analysis of intraplate seismic hazard," *Journal of Seismology and Earthquake Engineering*, vol. 7, 2005.

[22] S. Dardaei, H. Shakib, M. Khalaf Rezaei, and M. Mousavi, "Analytical and experimental seismic evaluation of confined masonry walls retrofitted by steel-fiber and polypropylene shotcrete," *Journal of Seismology and Earthquake Engineering*, vol. 16, no. 4, pp. 271–280, 2015.

[23] T. Qu and Q. Wang, "Method for solving bending vibration of underground pipeline under spatially varying seism," *Engineering Mechanics*, vol. 14, no. 03, pp. 88–96, 1997.